Modelling and simulation of fluid-flow and heat transfer in the convective zone of a power-generation boiler

Antonio Gómez, Norberto Fueyo, Luis Ignacio Díez

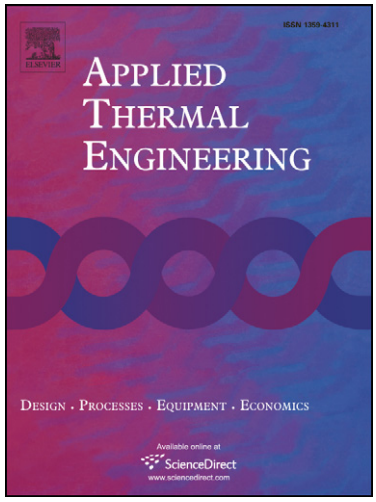

Modelling and simulation of fluid-flow and heat transfer in the convective zone of a power-generation boiler

Antonio Gómez, Norberto Fueyo, Luis Ignacio Díez

PII: S1359-4311(07)00176-7
DOI: 10.1016/j.applthermaleng.2007.04.019
Reference: ATE 2167

To appear in: *Applied Thermal Engineering*

Received Date: 26 September 2006
Revised Date: 26 April 2007
Accepted Date: 30 April 2007

Please cite this article as: A. Gómez, N. Fueyo, L.I. Díez, Modelling and simulation of fluid-flow and heat transfer in the convective zone of a power-generation boiler, *Applied Thermal Engineering* (2007), doi: 10.1016/j.applthermaleng.2007.04.019

Modelling and simulation of fluid-flow and heat transfer in the convective zone of a power-generation boiler

Antonio Gómez, Norberto Fueyo*

Fluid Mechanics Group, CPS, Universidad de Zaragoza, María de Luna 3, 50018 Zaragoza, Spain

Luis Ignacio Díez,

Fundación CIRCE, María de Luna 3, 50018 Zaragoza, Spain

Abstract

The convective zone of a power-station boiler is a complex piece of engineering equipment, which comprises a multiplicity of inter-connected heat-exchanging elements.

This paper presents a mathematical model of the convective zone, which allows for the calculation of the shell-side flow and the shell-side, tube-side and tube-wall, thermal fields, and of the shell-tube heat-exchange. The model is solved using conventional CFD techniques, in which the individual tubes are treated as sub-grid features. A geometrical model is used to describe the multiplicity of heat-exchanging structures, and the interconnections between them.

The CFD model is first validated by comparison with simple heat-exchanger geometries which can be solved with analytical methods, and then applied to an actual 350 MW (e) power-station boiler.

Key words:
Heat exchangers, power station boiler, convective zone, heat transfer, CFD, modelling

* Corresponding author; Norberto.Fueyo@unizar.es

1 Introduction

The shell-and-tube heat-exchanger is a ubiquitous piece of equipment in the power-generation and processes industries. In this type of heat exchanger, heat is transferred to (or from) a fluid flowing through a tube bundle from (or to) another fluid which flows around the tubes through the shell. Both fluids are everywhere separated by the tube wall (usually metal-made) and never become in direct contact.

The convective zone of a power-station boiler is a complex assembly of interconnected heat exchangers. Around 50% of the cycle heat generated in the boiler may be transferred in this zone, and hence the interest of the modelling of fluid flow and heat transfer. An accurate computer model can provide convenient and economical assistance in the design and in the operation of the convective zone, and can contribute significantly to the improvement of efficiency and durability. For the modelling to be accurate enough, a desirable feature of the model should be the ability to calculate simultaneously the (spatially-varying) temperature of both the shell and the tube fluids.

The modelling of shell-and-tube heat exchangers using Computational Fluid Dynamics techniques dates back to the early days of the discipline. It is difficult therefore to trace it to a seminal paper; however, the technique described in the one by Patankar and Spalding [1] was perhaps the first one capable of calculating simultaneously the thermal fields in both fluids and in the tube metal, and can be regarded as the framework from which successive contributions were developed.

A literature survey, however, shows that most of the published CFD-type simulations of large, shell-and-tube heat-exchangers pay much attention to the prediction of the aerodynamics (such as flow distribution or pressure losses), but fewer contributions can be found in which the thermal fields and heat transfer are also considered. This is the case in the early paper by Rhodes and Carlucci [2], which reports the first aerodynamic calculation of a model heat exchanger, and a comparison with experimental measurements. Despite the crude geometrical representation and discretisation, due to the limitations imposed by the computers available at the time, the mathematical model had many of the features still used nowadays for calculating the tube-bundle aerodynamic performance, such as the use of porosities, friction factors and effective viscosities to represent the effect of the tube bundle on momentum transport. The problem was later revisited by Theodossiou et al [3].

The simulation of power-plant condensers, which for the purpose of this paper can be regarded as a derivative of the heat exchanger, has attracted much attention in recent years. One of the most comprehensive three-dimensional

models is that used by Zhang et al [4], Zhang and Zhang [5] and Zhang and Bokil [6] for power-plant condensers, albeit the tube-side fluid is treated in a less general manner than that employed in this paper. Ormiston et al [7] [8] provide a literature survey of recent CFD models of power-plant condensers, as well as some modifications to the solution algorithm which can lead to better convergence behaviour. Prithiviraj and Andrews [9] [10] reformulate the finite-volume equations for the tube bundle using control-volume integrals of the model equations. The treatment of the tube-side enthalpy is again rather simple, since the condensers considered in their paper are single-pass ones.

No previous multi-dimensional simulations of the fluid flow and heat transfer in the convective zone of a power-station boiler, addressing both the shell-side and the tube-side fields have been traced in the open literature. The paper by Tu et al [11] addresses the CFD modelling of the fly-ash flow (without heat transfer) in power-utility boilers (including both the furnace and convective section) using Eulerian-Eulerian models. However, the emphasis is placed on the multi-phase, gas-particle model, and the representation of the convective section appears to be a simplified one. Coelho [12] has reported results from a CFD model of a boiler similar to the present one, but, unlike this work, the modelling is restricted to the shell side, and either the tube-side temperature is assumed or the overall heat transfer in a tube bank is known and distributed along the bank. Diez et al [13] address the modelling of the same boiler as featured in this work, but using a zonal method for the gas flow and lumped-parameter heat-exchanger network for the tube-side, together with CFD calculations of the combustion chamber to provide inlet conditions for the zonal model. Such a simplified model, it is argued, has the attractive merit of being usable on line. A similar method is used by Niu and Wong [14]. Huang et al [15] model the combustion chamber and heat exchanger of a domestic boiler; although few details of the mathematical model and numerical procedure are given, the method employed is probably similar to the one used in the present work.

This paper presents a mathematical model that can be used for the CFD simulation of fluid flow and heat transfer in the convective section of power-station boilers. The model, which builds on the method by Patankar and Spalding [1], represents the tubes as subgrid features; the meshing of individual tubes or periodically-repeating tube-arrays, while useful to improve the design of tube banks or to calculate their heat-exchanging or aerodynamic performance, such as pressure losses (see, eg, [16]), is computationally impractical for complex arrays of interconnected banks. The present model, on the other hand, allows for the simultaneous calculation of the shell-side, tube-side and metal thermal fields even when several interconnected heat exchangers have to be considered, as it is the case in power-station boilers.

2 Conservation equations

The present mathematical model can be best viewed as representing three "superimposed" spaces or "worlds", which coexist in physical space: the shell-side of the heat exchanger, the tube side and the metal. Conservation equations are solved for the relevant magnitudes in these three spaces, and include the appropriate exchange terms between them (eg, heat transfer).

Thus, for the shell-side, the relevant equations are continuity, momentum and enthalpy conservation. The continuity equation is:

$$\frac{\partial \epsilon_s \rho_s}{\partial t} + \nabla \cdot (\epsilon_s \rho_s \vec{v}_s) = 0 \tag{1}$$

where ϵ_s is the void fraction, *ie* the fraction of local space available to the shell-side fluid; ρ_s is the shell-fluid density; and $\vec{v}_s$ is the shell-fluid interstitial-velocity vector.

The shell-side-momentum equation is:

$$\frac{\partial \left(\epsilon_s \rho_s \vec{v}_s\right)}{\partial t} + \nabla \cdot (\epsilon_s \rho_s \vec{v}_s \vec{v}_s) - \nabla \cdot (\epsilon_s \mu_s \nabla \vec{v}_s) = -\epsilon_s \nabla P - \vec{F} \tag{2}$$

where μ_s is either the molecular viscosity (if the flow is laminar) or an effective (molecular plus turbulent) one if the flow is turbulent and an eddy-viscosity model is used; P is the pressure; and $\vec{F}$ is a friction term (specified below) that accounts for the pressure losses in the tube bank.

The shell-side-enthalpy (h_s) equation reads:

$$\frac{\partial \left(\epsilon_s \rho_s h_s\right)}{\partial t} + \nabla \cdot (\epsilon_s \rho_s \vec{v}_s h_s) - \nabla \cdot (\epsilon_s \Gamma_s \nabla h_s) = \alpha_{s \to w} \left(T_w - T_s\right) \tag{3}$$

where Γ_s is a diffusion coefficient; $\alpha_{s \to w}$ is a volumetric heat transfer coefficient from the shell fluid to the tube wall, with units W/m^3K; T_s is the local shell-fluid temperature; and T_w is the local tube-wall temperature. The use of a volumetric heat-transfer coefficient in this equation is required for dimensional reasons; it is calculated from the usual, per-unit-surface one using the ratio of tube surface to shell volume as detailed below. Other heat sources, such viscous heating or radiative heat-exchange, have been neglected in this equation.

If the flow in the shell side is turbulent, as it is usually the case, the above equations can be interpreted as being Favre-averaged. Then, if suitable eddy-viscosity turbulence model is used to close the unknown correlations, μ_s can be regarded as an effective shell-side viscosity, and Γ_s as an effective shell-side Prandtl number for h_s. Both can be calculated from the model parameters. The flow in utility boiler is clearly turbulent; in the application shown in

Section 6 below, the Reynolds number based on an average velocity and a boiler transversal dimension is in excess of 500,000. Turbulence in such a highly complex physical domain is correspondingly a complex issue. Given the impossibility to mesh the individual tubes in the banks, we have resorted to the use of a $k-\epsilon$ turbulence model, with some modifications to impose a length scale within the tube bank. While more sophisticated turbulence models are available, their use for the problem addressed in this paper does not justify the substantial additional computational expense, since the tube bank is nevertheless represented as a subgrid feature.

In the tube side, the flow is considered (locally) one-directional (*viz* in the direction of the tube orientation), which allows to obtain the local mass-flow rate by simple geometrical calculations (see below). Regarding the tube-side momentum equations, their only use would be to calculate tube-side head losses. However, if head losses in the tube-side circuit are quantity of interest, they can be calculated using simpler alternative methods, e.g. pipe-flow formulae. Thus, in the current application, the tube-side momentum equations are not required. The only relevant conservation equation for the tube side is therefore the one for enthalpy (h_t), which reads:

$$\frac{\partial\left(\epsilon_t \rho_t h_t\right)}{\partial t} + \nabla \cdot \left(\epsilon_t \rho_t \vec{v}_t h_t\right) = \alpha_{t\to w}\left(T_w - T_t\right) \tag{4}$$

where ϵ_t is the fraction of local space occupied by the tube-side fluid; $\vec{v}_t$ is the (one-directional) tube-side-fluid velocity vector; $\alpha_{t\to w}$ is a volumetric heat-transfer coefficient (from the shell fluid to the tube wall), with units W/m^3K; and T_t is the (bulk) tube-side-fluid temperature.

Streamwise heat conduction (molecular or turbulent) has been neglected in the above equation, since in all cases it will be much less important than convection. (Cross-stream conduction is accounted for in the volumetric heat-transfer coefficient $\alpha_{t\to w}$).

Finally, for the metal (the tube wall), the only relevant equation is the energy-conservation one, which, neglecting axial heat-conduction, reads:

$$\frac{\partial\left(\epsilon_w \rho_w h_w\right)}{\partial t} = \alpha_{s\to w}\left(T_s - T_w\right) + \alpha_{t\to w}\left(T_t - T_w\right) \tag{5}$$

where ϵ_w is the fraction of local space occupied by the tube wall.

An alternative framework to that presented here for addressing the space-sharing feature of the flow under consideration is the use of different computational spaces for each of the "co-existing worlds". Beale and Zhubrin [17] apply this concept in their simulation of Solid Oxide Fuel Cells.

3 Auxiliary equations

3.1 Pressure losses

Pressure losses ($\vec{F}$ in equation (2)) are calculated by means of friction factors ξ, as follows:

$$F_i = \xi_{u_i} \rho_s u_i U \tag{6}$$

where u_i is the i^{th} component of the velocity vector, U is the absolute value of the velocity vector, and the friction factors ξ_{u_i} are calculated similarly to Rhodes and Carlucci [2] as:

$$\xi_{u_i} = 2 \left(\frac{f_\parallel}{\overline{P}} \right) \left(\frac{1 - \epsilon_s}{1 - \epsilon} \right) \tag{7}$$

for the parallel-flow direction and

$$\xi_{u_i} = 2 \left(\frac{f_\perp}{P} \right) \left(\frac{P \epsilon_s}{P - D_o} \right)^2 \left(\frac{1 - \epsilon_s}{1 - \epsilon} \right) \tag{8}$$

for the crossflow direction.

In equations (7) and (8), the factors $f_\parallel$ and $f_\perp$ are functions of the local Reynolds number [2]; P is the tube pitch in the cross-flow direction; $\overline{P}$ is an average pitch; D_o is the tube outer-diameter; ϵ_s is the local void fraction, and ϵ is the void fraction in the local tube-bank. These both can be readily calculated from geometrical data.

An alternative means of combining the contributions from the principal directions to the pressure loss is the tensorial approach suggested by Butterworth [18].

3.2 Heat-transfer coefficients

For the calculation of the volumetric heat transfer coefficient $\alpha_{t \to w}$ in equation (4), we first compute the (per-unit-surface) heat-transfer coefficient $\alpha''_{t \to w}$ by considering the heat-transfer resistances due to heat convection and fouling:

$$\frac{1}{\alpha''_{t \to w}} = R_t + R_{ft} \tag{9}$$

The convection resistance R_t is obtained using a Nusselt-number correlation:

$$\frac{1}{R_t} = \frac{Nu\ k_t}{D_i} \tag{10}$$

with k_t being the tube-side-fluid thermal-conductivity and $Nu = 0.023 Re_t^{0.8} Pr_t^{0.4}$ ([19]). Transport and thermodynamic properties for this correlation are calculated at the local tube temperature, which is an output from the model.

Finally, the dimensions of $\alpha_{t\to w}$ in equations (4) and (5), *ie* W/m^3K, are recovered from those of $\alpha''_{t\to w}$ (W/m^2K) by multiplying the coefficient by the surface-to-volume ratio in the bank, *ie* by the local ratio of heat-exchanging surface S to physical volume V:

$$\alpha_{t\to w} = \alpha''_{t\to w}\frac{S}{V} \tag{11}$$

The shell-to-wall heat-transfer coefficient $\alpha_{s\to w}$ is calculated in a similar manner:

$$\frac{1}{\alpha''_{s\to w}} = R_s + R_{fs} \tag{12}$$

with the resistance coefficient R_s now calculated using the correlation proposed by Zhukauskas [20] for the Nusselt number:

$$Nu = C Re_s^m\ Pr_s^{0.36}\left(\frac{Pr_s}{Pr_w}\right)^{1/4} \tag{13}$$

Here, the Reynolds number is calculated with the tube external diameter and the maximum gas velocity within the tube bank. The gas Prandtl numbers Pr_s and Pr_w are calculated respectively at the local gas temperature and at the wall temperature, both obtained from the model.

The constants C and m depend on tube-bank configuration and Reynolds number; see Zhukauskas [20] for details and for the range of validity for the correlation.

It is difficult to reliably calculate the shell-side fouling-resistance from other flow parameters, despite past and on-going research efforts on fouling modelling and prediction (Erickson et al [21]; Zibas and Idem, [22]; Bergeles et al [23]; Wang and Harb [24]; Isdale et al [25]; Kaer et al [26]). In the present work, empirical values, calculated from plant data, will be used.

3.3 Turbulence

The modification of the turbulence in the presence of tube bundles has been addressed by several authors in the past. When eddy-viscosity models are used,

a common approach is to modify the turbulent viscosity in the tube bundle, *eg* by using a length scale (typically proportional to the clearance between tubes) and a velocity fluctuation to obtain an effective viscosity or thermal diffusivity (Rhodes and Carlucci [2]). Another approach (see *eg* Prithiviraj and Andrews [9]) modifies the source term in the k and ϵ equations to account for the enhanced production and dissipation of turbulence in the tube bundle.

In this work, a version of the first approach is used. The gas effective-viscosity for points located within the tube bundle is calculated considering that the tube clearance is a characteristic length scale l. For the fluctuating velocity, $k^{1/2}$ is used. Thus:

$$\mu_T = C_\mu \rho_s l k^{1/2} \tag{14}$$

where C_μ is a standard constant in the k-ϵ model [27]; the turbulent kinetic energy k is calculated from the standard equation [27]; and the characteristic length-scale l is set within the tube bundle as $l = \overline{P} - D_o$, with $\overline{P}$ being the average local pitch.

Outside the tube bundle, the effective viscosity is calculated as usual with the Prandtl-Kolmogorov formula and the k-ϵ model.

The effective diffusivity Γ_s in equation (3) is calculated as $\Gamma_s = \mu_T / Pr_s$. The turbulent Prandlt number for the shell-side enthalpy is taken as $Pr_s = 0.9$.

3.4 Steam properties

The tube-side of the convective zone often consists of steam in greatly-differing thermodynamic conditions. Thus, properties such as density, thermal conductivity or specific heat cannot be regarded as constant, and for an accurate calculation of shell-to-tube heat transfer they must be computed as a function of the local temperature and pressure. In this work, the IAPWS-IF97 formulation for water and steam [28] has been attached to the simulation code for this purpose.

4 Geometrical description

One of the main difficulties in simulating heat exchangers and convective zones is often their geometrical complexity, since they are often composed of a large number of interconnected tube banks. This is certainly true of the convective zone of a power-station boiler.

The approach embodied in the equations introduced above implies the treat-

ment of tubes as subgrid features. This somehow alleviates the problem, since it circumvents the need for meshing individual tubes; but some significant difficulties still remain, and this section describes how they have been addressed in the present model.

The geometrical description used in this model considers essentially two types of element: tube banks and manifolds. The tube bank is the main heat-exchanging item. They can be "two-dimensional" (ie, a single plane of tubes) or "three dimensional". In either case, they can additionally be present in the form of "arrays" of identical structures regularly arranged in space. Tube banks are characterised by geometrical, physical and topological properties. Among the geometrical properties, the main relevant ones are pitch, external and internal diameters, position and dimensions. The physical properties include all the tube-side-fluid properties, the tube material (and hence its properties), and the mass-flow rate per tube. The all-important topological properties are two: the flow direction within the tubes, by reference to the simulation axes, and the bank connectivity, *ie* to which other bank(s) each bank is connected and how.

One type of such connection (but not the only one) is the manifold (or header). This is defined as a virtual element (*ie* without a geometrical representation in the model) where the tube-side flow from one or several banks is collected, and probably mixed and distributed to other banks. The "inlet" manifold is a special type of manifold, which is used to distribute to the appropriate tube banks the tube-side fluid arriving from other plant devices not included in the simulation (eg, the steam fed to the reheater from the turbine). Several inlet manifolds are allowed in the model, so that several independent (not interconnected) steam and water circuits can be present in the calculation, as is the case in power-generation boilers.

5 Solution

5.1 Simultaneous treatment of the three phases

Equations (1)-(5) can be discretised and solved using any CFD technique. The solution procedure is however complicated by the presence of three distinct phases: the shell-side gas-phase; the tube-side vapor- (or liquid-) phase; and the metal, solid phase. An economical and easy-to-implement method can be used when quasi-steady-state is assumed in the metal-side enthalpy-equation (5). In these circumstances, the left-hand side of the equation vanishes, and the equation can be used to calculate the metal temperature:

$$T_w = \frac{\alpha_{s\to w} T_s + \alpha_{t\to w} T_t}{\alpha_{s\to w} + \alpha_{t\to w}} \tag{15}$$

This value for T_w can then be used in equations (3) and (4).

A further simplification in the numerical solution can be achieved if the tube-side flow in the heat-exchanging banks is always considered to be one-directional, and aligned with any of the mesh directions. Then equation (4) for h_t can be discretised as:

$$\begin{aligned} &\frac{V_P}{\Delta t}\left(\rho_{tP} h_{tP} - \rho_{tT} h_{tT}\right) - \max\left[A_t u_{tw} \rho_{tW} h_{tW}, 0\right] + \\ &+ \max\left[-A_t u_{tw} \rho_{tP} h_{tP}, 0\right] + \max\left[A_t u_{te} \rho_{tE} h_{tE}, 0\right] - \\ &- \max\left[-A_t u_{te} \rho_{tP} h_{tP}, 0\right] = \frac{\alpha_{t\to w}}{Cp_t} V_P \left(h^w_{tP} - h_{tP}\right) \end{aligned} \tag{16}$$

where it has been assumed (without loss of generality) that the tube is oriented in the x (West-to-East) direction (see figure 1); the max function expresses the upwinding practice for the enclosed quantity (*ie*, the value convected into the cell through the cell face is the value in the upwind cell center); A_t is the total cross-sectional area of the tubes in the cell; $g = A_t u_{tP} \rho_{tW}$ and similar terms are the tube-side mass-flow-rate per cell, constant along the cells in the same tube bank on mass-conservation grounds; and V_P is the cell volume. Compared to the differential equation (4), the right-hand-side uses enthalpies, rather than temperatures. Thus, $h_t = Cp_t T_t$ is the tube-side-fluid enthalpy, and $h^w_t = Cp_t T_w$ is the tube-side-fluid enthalpy at the wall temperature.

Since the tube-side mass-flow-rate g is known for each cell in the bank from the geometrical model, equation (16) can be cast into simple, source-only, linear equation in the form:

$$0 = S_1 - S_2 h_{tP} \tag{17}$$

with S_1 and S_2 being appropriate coefficients, variable from cell to cell, but not explicitly dependent on h_{tP}. After this manipulation, the convective term in equation (16) has been transferred to the source term in (17); and, since the latter does not (formally) have a convection term, it can be easily solved alongside the discretised versions of the shell-side equations (1), (2) and (3), which in general of course do have a convection term.

5.2 Tube-side mass-conservation

The model conservation equations do not include a three-dimensional, tube-side continuity-equation because the flow in each tube is one-directional and

confined. The geometrical model thus ensures mass conservation within the same tube bank, and also when a bank is directly linked to another one. However, some provisions must be made to calculate the flow distribution when a manifold is fed by, and in turn feeds, several tube banks.

The mass-flow rate m_i through element i (be it a tube bank or a manifold) is given by the equation

$$m_i = \sum_{j \neq i} m_j \frac{\delta_{ij}}{n_j} + b_i \tag{18}$$

where m_j is the mass-flow rate through element j, δ_{ij} is 1 if element i feeds element j and 0 otherwise, n_j is the number of (equal) elements fed from j, and b_i is the mass flow-rate if i is an inlet manifold, and 0 otherwise.

Equation (18) is cast into a matrix form $[A][m] = [b]$, which is solved by LU decomposition to calculate the vector of the unknown mass-flow rates $[m]$.

5.3 Numerical details

The equations and algorithms described above have been coded by the authors into the finite-volume CFD-code PHOENICS ([29]); version 2.2 has been used. For accuracy and efficiency, structured, Cartesian grids are employed, and porosities are selectively used were needed to account of the fraction of local space occupied by tubes and thus unavailable to the flue gas. Second-order interpolation schemes are used for shell-side velocities, turbulence statistics and enthalpy.

A typical discretisation for a convective zone, such as that shown in Results section below, involved around 700,000 cells, and takes around 10 hours CPU time to converge on a Pentium IV at 3 GHz. A parametric analysis was performed with a finer grid of 1.1 million cells to confirm that results are grid independent.

6 Results

6.1 Validation tests

Validation tests have been performed mainly in respect of two different aspects of the model. The first aspect is the correct working of the several features of the geometrical model, such as the different connectivity options and the

conservation of overall tube-side-fluid mass. These tests will not be reported here.

The second validation initiative has consisted in predicting of the overall heat-transfer rates in geometrically-simple configurations. The results of this validation exercise are reported in this section.

The simple configurations considered are single-pass, cross-flow heat exchangers, which can be analysed alternatively using either the Log Mean Temperature Difference (LMTD) method or the effectiveness-NTU (Number of Transfer Units) method [30]. While these alternative theoretical methods are also approximations, the similarity of the results with both the numerical and theoretical approaches adds confidence in the accuracy of the former.

A general schematic of the configuration is represented (in cross-section) in figure 2, where the main heat-exchanger and flow parameters are shown. Table 2 presents the values of these parameters for the different cases used in the validation. The test cases include a range of tube diameters, pitch values, gas velocities and gas and tube-side inlet temperatures. Cases with constant and variable tube-side temperature are both considered.

Validation results are presented in table 3, and show a good agreement between both calculation methods. For instance, discrepancies in outlet temperatures in both calculation methods are normally around 1%, with only one case (case 4) yielding differences around 4%.

6.2 Convective-zone modelling

The model has been applied to the simulation of the convective zone of a power station boiler. This is one of the three 350 MW(e), wall-fired boilers of the Teruel power station located at Andorra (Teruel, Spain). The unit is a sub-critical coal-fired utility boiler, with natural circulation and balanced draft. The boiler possesses three stages of superheat, a single reheat a two economisers. The combustion and heat transfer in the furnace zone has been already investigated numerically in the past by one of the present authors [31].

A schematic of the convective zone is shown in figure 3. After leaving the furnace, the flue gas flows across radiant superheater (wing walls) and final superheater (FS). Downstream the final superheater, the gas enters the convective zone separated in two parallel passes. Two independent water-steam circuits can be found in the boiler. In the shorter one, steam is drawn from the high-pressure turbine through the reheater (RH) and sent back to the power cycle. The other one is the main water-steam circuit. The water is fed into this circuit through the lower economiser (LE) and then through

the upper economiser (UE). From there, the hot water is sent to the drum separator, where liquid water and steam are at equilibrium conditions. The liquid phase from the drum circulates through down-comers to the furnace water-walls where the phase change from liquid to steam takes place using the heat released in the combustion zone, and then returns as a two-phase mixture to the drum. From there, dry steam is distributed through the tubes that line the ceiling and walls of the convective zone (which therefore serve as a preliminary superheater), and then collected in a manifold and circulated successively through the primary superheater (PS), the wing walls (WW) and the final superheater (FS). From this last heat exchanger, the steam is sent to the high-pressure turbine. The gas flow-rates through the parallel passes of the convective section are adjusted to maintain the steam temperature at reheater outlet by means of regulating dampers, located under the lower economiser. The reheater is located in the rear pass of the boiler, whereas the primary superheater and upper economiser are located in the frontal one. Aside from the main gas outlet at the cold end of the lower economiser, there is a secondary extraction of hot gases (between the reheater and the lower economiser) to regulate the gas temperature at each of air preheater inlets.

Some plant measurements in the convective zone are available, and will be used for comparison with computed results in this section. This type of utility boilers are conventionally instrumented, providing of course enough measurements for their safe operation and control. However, such information is neither complete nor reliable enough to be used in the validation of thermo-fluid-dynamical models. In part to remedy this situation, a plan for the improvement and extension of instruments and measurement procedures was designed and implemented in this case-study boiler. The rationale and details of this plan can be found in [32]. As for the variables used for validation in the present paper, discussed in this section, a grid of eight gas thermocouples was installed at the lower economiser outlet, and six water and steam thermocouples were installed at upper economiser, primary superheater and reheater outlets; the former were installed to reduce the uncertainty due to temperature stratification in the flow and the latter to obtain more reliable data by taking additional measurements at ends of the external headers. Serious technical problems arose when attempting to instrument headers located inside the boiler enclosure. Thermowells equipped with armoured outfit can be installed in this situation, but this possibility was discarded owing to doubts about integrity of the pressure circuit. In consequence, the water temperature at lower economiser outlet (*ie* upper economiser inlet) and the steam temperature at primary superheater inlet were not measured.

The operating conditions change considerably depending on the load, or fraction of the nominal power at which the boiler operates. For instance, the pressure at economiser inlet varies from 166 bar to 183 bar, and the range of temperatures at the reheater inlet from 595 K to 640 K. Table 4 presents

the operating conditions for different loads, which are used as input data in the simulations carried out to validate the model. Most of these data are directly-available measurements, but some of them are indirectly estimated using other operating data. This is the case of gas mass-flow-rate (obtained by closing the overall mass balance in the boiler), steam mass-flow-rate leaving the drum (mass balance in the main steam circuit) and steam mass-flow-rate at reheater inlet (mass balance considering the high-pressure extractions to the water heaters in the cycle).

For these convective-zone calculations, tube-side heat-transfer resistances are neglected. For the shell side, values calculated from the application of semi-empirical heat-transfer models are used. The direct measurement of ash fouling rates in this type of equipment is technically unfeasible, and therefore one has to resort to indirect thermal calculations. In this case, a semi-empirical approach was proposed in [33], aiming at the on-line estimation of these thermal resistances. The method basically consists in the formulation of a lumped model for large heat exchangers, such as those found in utility boilers, coupled with energy balances in a separated per-section analysis. Typical mean values for the shell-side heat-transfer resistances, calculated in this way to account for ash fouling, have been used in the CFD simulations: for the reheater $R_{fs} = 0.00459\ Km^2/W$; for the primary superheater $R_{fs} = 0.004163\ Km^2/W$; for the lower economiser $R_{fs} = 0.00173\ Km^2/W$; for the upper economiser $R_{fs} = 0.002062\ Km^2/W$.

Figure 4 is a three-dimensional view of the geometry as generated directly from the geometrical model (tube banks are represented as solid boxes for simplicity, but fluid flow is of course allowed through them in the model). The simulation domain starts at the end of the combustion zone, just under the "nose", where uniform velocity and temperature profiles are presumed. (The convective-zone model can be coupled with models for the combustion zone, which would allow this presumption to be relaxed by using calculated results in the absence of detailed experimental data.)

Figures 5 and 6 represent the shell-side temperature and (superimposed) the shell-side velocity vectors in a 2D view of the mid-plane for 60% and 100% load respectively, showing how the gas temperature gradually decreases along the flow path. The flow pattern is very similar in both cases, as it can be expected; and the temperature map is also similar, albeit the temperatures are lower for the lower load as expected.

Figures 7 and 8 are the corresponding tube-side temperatures. The interconnection of the tube banks in both steam circuits is apparent from the gradual change in the tube-side temperature even when the interconnected banks are not contiguous in physical space.

The graph in figure 9 compares the total heat heat exchanged in the convective zone (reheater, primary superheater, lower and upper economiser) with the measured one for several loads. The agreement is generally good, but the case for 100% load shows a more significant discrepancy, with the model tending to follow more closely the linear behaviour found for lower loads. Figure 10 is the corresponding graph for the calculated and measured average outlet temperatures of water or steam in the upper economiser, reheater and primary superheater outlets, and the computed and measured mean temperature of the gas at the outlet of the convective zone. There is a good agreement in both figures between calculated and experimental data.

7 Conclusions and future work

The present paper has introduced a means of simultaneously calculating the shell-side flow-field, the shell-side and tube-side thermal fields and the tube-wall temperature in the convective zone of a power station boiler. The model allows for several arbitrarily-interconnected heat-exchanging elements to be simulated in a flexible manner. The model has been validated with the simulations of a real power-station convective zone for different loads, and the agreement between calculated and plant data has been satisfactory. These results are indicative of the capability of the model to deal with the different operating conditions of a real plant and the its usefulness in the study of the performance of convective zones.

The model described here can be extended with relative ease to account for additional physical processes. Firstly, heat transfer by radiation is bound to relevant in the convective surfaces which are exposed to the flame. Heat transfer by radiation can be accounted for in the model either as a direct flame-to-surface phenomenon (*eg* by use of viewfactors), or by considering the gas as a participating media, by use of a full radiation model. In the absence of other data, incoming radiation from the flame zone to the convective one can be estimated from furnace-combustion models. These can be usefully coupled to the present convective-zone model to obtain other relevant boundary conditions which are difficult to obtain experimentally (eg, velocity or temperature distributions on the convective-zone inlet-plane). A two-way coupling would allow, among other things, to account for the possible effect of pressure losses in the convective zone on the flow pattern in the furnace.

Shell-side fouling has been modelled in the present work using experimental values for the associated heat-transfer resistance. Research work, such as that cited in the introduction, can be with some effort integrated in the model to simulate the motion of the fly-ash in the convective section, the build-up of deposits, and their impact on heat transfer. Work along these lines has been

recently published by Kær et al [26].

In respect of the tube-side submodels, an extension can be devised to calculate head losses in the tube-side circuits. The flow distribution from the manifolds to the individual tubes can then be calculated, if required, in a more accurate manner using this information.

8 Acknowledgements

This work was partly supported by the European Union under Contract ECSC 7220/ED/096 to Grupo ENDESA. The cooperation of Dr Juan Francisco Gonzalez and Mess Enrique Perez and Mariano Lacarta of Grupo ENDESA is gratefully acknowledged. We also thank CHAM (London, UK), for granting us the use of their PHOENICS CFD code, in which the models outlined in this paper have been coded by the authors.

9 Nomenclature

A_t	Cross-sectional surface-area of tubes in a cell (m^2)
b_i	Inlet mass-flow rate through element i (if a manifold) (kg/s)
Cp_t	Specific heat of tube-side fluid (J/kgK)
C_μ	Constant in the $k-\epsilon$ turbulence model
D_i	Inner tube diameter (m)
D_o	Outer tube diameter (m)
F_i	i^{th} component of friction term (kg/m^2s^2)
$\vec{F}$	Friction term accounting for shell-side pressure-losses in the tube bank (kg/m^2s^2)
g	Tube-side mass-flow-rate per cell (kg/s)
h_s, h_t, h_w	Specific enthalpy of shell-side fluid, tube-side fluid and tube wall respectively (J/kg)
h_{tE}	Specific enthalpy of tube-side fluid in the East cell (J/kg)
h_{tP}	Specific enthalpy of tube-side fluid in the current cell (J/kg)

h_{tT}	Specific enthalpy of tube-side fluid at the previous time-step (J/kg)
h_{tW}	Specific enthalpy of tube-side fluid in the West cell (J/kg)
h_t^w	Specific enthalpy of tube-side fluid at the tube-wall temperature (J/kg)
k	Turbulent kinetic energy (m^2/s^2)
k_t	Thermal conductivity of tube-side fluid (W/mK)
l	Characteristic length scale in the tube bundle (m)
m_i	Mass flow rate through element i (kg/s)
Nu	Nusselt number (–)
n_j	Number of elements fed from element j (–)
P	Pressure (Pa)
P	Tube pitch in the cross flow direction (m)
$\overline{P}$	Average pitch in the tube bundle (m)
Pr_s, Pr_w	Prandtl numbers of shell-side fluid calculated at the local fluid temperature and at the wall temperature respectively
Pr_t	Prandtl number of tube-side fluid calculated at the local fluid temperature
R_{fs}	Shell-side fouling resistance (m^2K/W)
R_{ft}	Tube-side fouling resistance (m^2K/W)
R_s	Shell-side convection resistance (m^2K/W)
R_t	Tube-side convection resistance (m^2K/W)
Re_s, Re_t	Local Reynolds number of the shell-side and tube-side fluids
S/V	Ratio of tube surface-area to volume in the bank (m^2/m^3)
t	Time (s)
T_s, T_t, T_w	Shell-side-fluid temperature, tube-side-fluid temperature and tube-wall temperature (K)
u_i	i^{th} component of velocity vector (m/s)
u_{te}	Tube-side-fluid velocity across the East cell-face (m/s)
u_{tw}	Tube-side-fluid velocity across the West cell-face (m/s)

U	Absolute value of velocity vector (m/s)
$\vec{v_s}$	Shell-side-fluid velocity-vector (m/s)
$\vec{v_t}$	Tube-side-fluid velocity-vector (m/s)
V_P	Volume of cell P (m^3)

Greek Letters

$\alpha_{t\to w}$	Volumetric heat-transfer coefficient from the tube-side fluid to the tube wall (W/m^3K)
$\alpha_{s\to w}$	Volumetric heat-transfer coefficient from the shell-side fluid to the tube wall (W/m^3K)
$\alpha^{"}_{s\to w}$	Heat-transfer coefficient from the tube-side fluid to the tube wall (W/m^2K)
$\alpha^{"}_{t\to w}$	Heat-transfer coefficient from the tube-side fluid to the tube wall (W/m^2K)
δ_{ij}	Connectivity parameter (=1 if element i feeds element j and 0 otherwise)
Δt	Time interval (s)
ϵ	Dissipation rate of the turbulent kinetic energy (m^2/s^3)
ϵ_s	Fraction of local space occupied by the shell-side fluid
ϵ_t	Fraction of local space occupied by the tube-side fluid
ϵ_w	Fraction of local space occupied by the tube wall
Γ_s	Effective diffusivity in the shell-side enthalpy-equation (kg/ms)
μ_s	Molecular (dynamic) or effective (molecular plus turbulent) viscosity of the shell-side fluid (kg/ms)
μ_T	Turbulent viscosity of the shell-side fluid (kg/ms)
ρ_s, ρ_t, ρ_w	Density of shell-side fluid, tube-side fluid and tube wall respectively (kg/m^3)
ξ_{u_i}	Friction factor for the i^{th} component of velocity vector (m^{-1})

Subscripts

E	East cell
f	Fouling

P	Current cell
s	Shell-side fluid
t	Tube-side fluid
w	Tube wall
W	West cell

References

[1] S. V. Patankar, D. B. Spalding, A calculation procedure for the transient and steady-state behaviour of shell-and-tube heat exchangers, in: A. A. Afgan, E. U. Schluner (Eds.), Heat Exchangers: Design and Theory Sourcebook, 1974, pp. 155–176.

[2] D. B. Rhodes, L. N. Carlucci, Predicted and measured velocity distributions in a model heat exchager, in: International conference on numerical methods in Engineering, Canadian Nuclear Society and American Nuclear Society, 1983, pp. 935–948.

[3] V. M. Theodossiou, A. Sousa, L. Carlucci, Flow field predictions in a model heat exchanger, Computational Mechanics 3 (1988) 419–428.

[4] C. Zhang, A. C. M. Sousa, J. E. S. Venart, The numerical and experimental study of a power plant condenser, Journal of Heat Transfer 115 (1993) 435–445.

[5] C. Zhang, Y. Zhang, A quasi-three-dimensional approach to predict the performance of steam surface condensers, Journal of Energy Resources Technology 115 (1993) 213–220.

[6] A. Zhang, C.; Bokil, A quasi-three-dimensional approach to simulate the two-phase fluid flow and heat transfer in condensers, International Journal of Heat Mass Transfer 40 (15) (1997) 3537–3546.

[7] S. J. Ormiston, G. D. Raithby, L. N. Carlucci, Numerical modeling of power station steam condensers. part 1: Convergence behavior of a finite-volume model, Numerical Heat Transfer, Part B 27 (1) (1995) 81–102.

[8] S. J. Ormiston, G. D. Raithby, L. N. Carlucci, Numerical modeling of power station steam condensers. part 2: Improvement of solution behavior, Numerical Heat Transfer, Part B 27 (1) (1995) 103–125.

[9] M. Phrithiviraj, M. Andrews, Three-dimensional numerical simulation of shell-and-tube heat exchangers. Part I: Foundation and fluid mechanics, Numerical Heat Transfer, Part A 33 (8) (1998) 799–816.

[10] M. Phrithiviraj, M. Andrews, Three-dimensional numerical simulation of shell-and-tube heat exchangers. Part II: Heat transfer, Numerical Heat Transfer, Part A 33 (8) (1998) 817–828.

[11] J. Y. Tu, C. A. J. Fletcher, M. Behnia, Numerical modelling of three-dimensional fly-ash flow in power utility boilers, International Journal for Numerical Methods in Fluids 24 (1997) 787–807.

[12] P. J. Coelho, Mathematical modeling of the convection chamber of a utility boiler – an application, Numerical Heat transfer, Part A 36 (1999) 411–428.

[13] L. I. Diez, C. Cortes, A. Campo, Modelling of pulverized coal boilers: review and validation of on-line simulation techniques, Applied Thermal Engineering 25 (2005) 1516–1533.

[14] Z. Niu, K.-F. V. Wong, Adaptive simulation of boiler unit performance, Energy Conversion Management 39 (13) (1998) 1383–1394.

[15] L. Huang, W. J. X, T. G. Karayiannis, R. D. Matthews, Numerical predicion of high efficiency boiler heat exchanger performance, Applied Thermal Engineering 18 (1998) 1089–1099.

[16] A. Horvat, M. Leskovar, B. Mavko, Comparison of heat transfer conditions in tube bundle cross-flow for different tube shapes, International Journal of Heat and Mass Transfer 49 (2006) 1027–1038.

[17] S. B. Beale, S. V. Zhubrin, A distributed resistance analogy for solid oxide fuel cells, Numerical Heat Transfer, Part B 47 (2005) 573–591.

[18] D. Butterworth, The development of a model for three-dimensional flow in tube bundles, International Journal of Heat and Mass Transfer 21 (1977) 253–256.

[19] American Society of Heating, Refrigerating and Air Conditioning Engineers Inc, Atlanta, GA, ASHRAE Handbook, Fundamentals (1989).

[20] A. Zhukauskas, Heat transfer from tubes in crossflow, in: J. P. Harnett, T. F. Irvine (Eds.), Advances in Heat Transfer, Vol. 8, Academic Press, New York, 1972, pp. 93–160.

[21] T. Erickson, S. Allan, D. McCollor, J. Hurley, S. Srinivasachar, S. Kang, J. Baker, M. Morgan, S. Johnson, R. Borio, Modelling of fouling and slagging in coal-fired utility boilers, Fuel Processing Technology 44 (1995) 155–171.

[22] S. Zibas, S. Idem, Boiler heat transfer modeling using cems data with application to fouling analysis, in: ASME Joint Power Generation Conference, Vol. 30, 1996, pp. 655–661.

[23] G. Bergeles, D. Bouris, M. Yianneskis, S. Balabani, A. Kravaritis, S. Itskos, Effects of fouling on the efficiency of heat exchangers in lignite utility boilers, Applied Thermal Engineering 17 (8-10) (1997) 739–749.

[24] H. Wang, J. Harb, Modeling of ash deposition in large-scale combustion facilities burning pulverized coal, Prog. Energy Combust. Sci. 23 (1997) 267–282.

[25] J. Isdale, P. Mercier, J. Grillot, A. Mulholland, J. Gomatam, Integrated modelling of process heat transfer with combustion and fouling, Applied Thermal Engineering 17 (8-10) (1996) 751–762.

[26] S. Kær, L. Rosendahl, L. Baxter, Towards a CFD-based mechanistic deposit formation model for straw-fired boilers, Fuel 85 (2006) 833–848.

[27] B. E. Launder, D. B. Spalding, Mathematical Models of Turbulence, Academic Press, New York, 1972.

[28] W. Wagner, J. Cooper, A. Dittmann, J. Kijima, H.-J. Kretzschmar, A. Kruse, R. Mareš, K. Oguchi, H. Sato, I. Stocker, O. Šifner, Y. Takaishi, I. Tanishita, J. Trübenbach, T. Willkommen, The IAPWS Industrial Formulation 1997 for the thermodynamic properties of water and steam, Journal of Engineering for Gas Turbines and Power 122 (2000) 150–182.

[29] D. B. Spalding, A general purpose computer program for multi-dimensional one and two phase flow, Journal of Mathematics and Computers in Simulation 23 (1981) 265–276.

[30] F. P. Incropera, D. P. D. Witt, Fundamentals of Heat and Mass Transfer, 2nd Edition, John Wiley and Sons, 1985.

[31] N. Fueyo, J. Ballester, C. Dopazo, An Eulerian-Eulerian model of coal combustion, NOx formation and reburning, in: 12th Annual International Pittsburgh Coal Conference, 1995, pp. 1113–1116.

[32] L. I. Díez, C. Cortés, I. Arauzo, A. Valero, Combustion and heat transfer monitoring in large utility boilers, Int. J. Therm. Sci. 40 (2001) 489–496.

[33] C. Cortés, L. I. Díez, A. Campo, Modeling large-size boilers as a set of heat exchangers: tips and tricks, ASME HTD Combustion and Energy Systems 369 (4) (2001) 41–48.

Table 2
Validation cases. All cases solved with LMTD method, except Case 5 with effectiveness-NTU.

Case	L (m)	N_T $(--)$	N_L $(--)$	P_T (m)	P_L (m)	D (m)	V_∞ (m/s)	T_s^{in} (^oC)	T_s^{out} (^oC)	T_t^{in} (^oC)	T_t^{out} (^oC)
1	0.75	20	15	0.038	0.038	0.019	8	325	341.95	375	375
2	1.0	12	8	0.0285	0.057	0.019	7	293.15	303.8	328.15	328.15
3	1.0	14	14	0.015	0.015	0.01	5	298.15	344.21	373.15	373.15
4	1.0	5	20	0.02	0.02	0.01	10	1200	615	400	400
5	4.0	10	10	0.05	0.05	0.025	5	800	625	300	345.04

Table 3
Validation cases. Comparison of theoretical and simulation results.

Case	T_s^{out} (K) theor	T_s^{out} (K) simul	T_t^{out} (K) theor	T_t^{out} (K) simul	W (kW) theor	W (kW) simul	$\alpha''_{s\to w}$ (W/m2K) theor	$\alpha''_{s\to w}$ (W/m2K) simul
1	341.95	341.21	(Const)	(Const)	91.80	91.64	167.0	168.5
2	303.80	303.38	(Const)	(Const)	33.41	33.98	199	203.6
3	344.21	341.88	(Const)	(Const)	62.39	62.26	210	211.9
4	615	641	(Const)	(Const)	201.1	241.3	148.5	150.8
5	625.0	634.4	345.0	343.5	885.0	910.8	81.0	83.3

Table 4
Operating conditions for different loads (mfr = mass flow-rate)

Load	60%	75%	85%	95%	100%
Flue-gas mfr (kg/s)	256	313	360	402	440
Flue-gas inlet-temperature (K)	1300	1300	1300	1300	1300
Water mfr at economiser inlet (kg/s)	201	240	275	292	329
Water temperature at economiser inlet (K)	503	516	523	526	542
Water pressure at economiser inlet (bar)	166	170	173	179	183
Steam mfr at steam-drum outlet (kg/s)	148.2	193.6	230	268	284
Steam temperature at steam-drum outlet (K)	623	626	626	626	630
Steam pressure at steam-drum outlet (bar)	165	171	172	178	180
Steam mfr at reheater inlet (kg/s)	142	180.2	208	232	266
Steam temperature at reheater inlet (K)	595	612	620	627	640
Steam pressure at reheater inlet (bar)	24	30	34.5	40.5	42.2

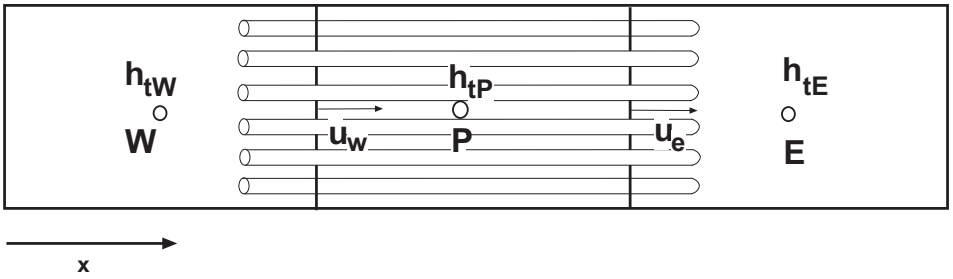

Fig. 1. Three-cell schematic showing the discretisation of the tube-side enthalpy equation (for tubes aligned with the x direction)

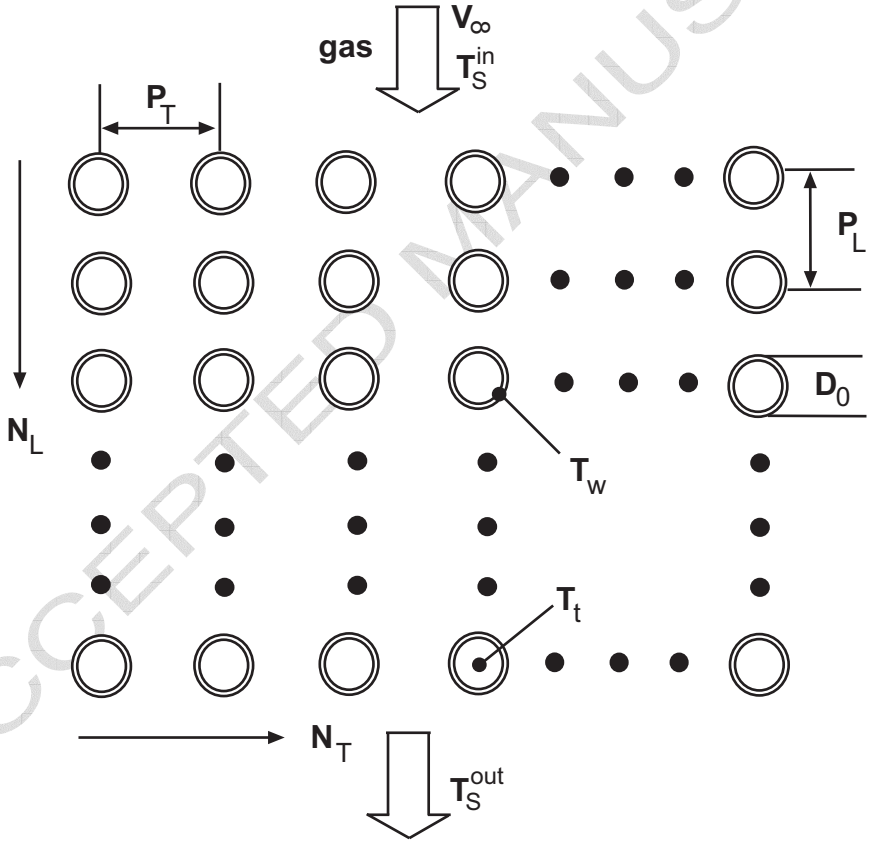

Fig. 2. Schematic of the two-dimensional heat-exchanger, showing the main dimensions and parameters

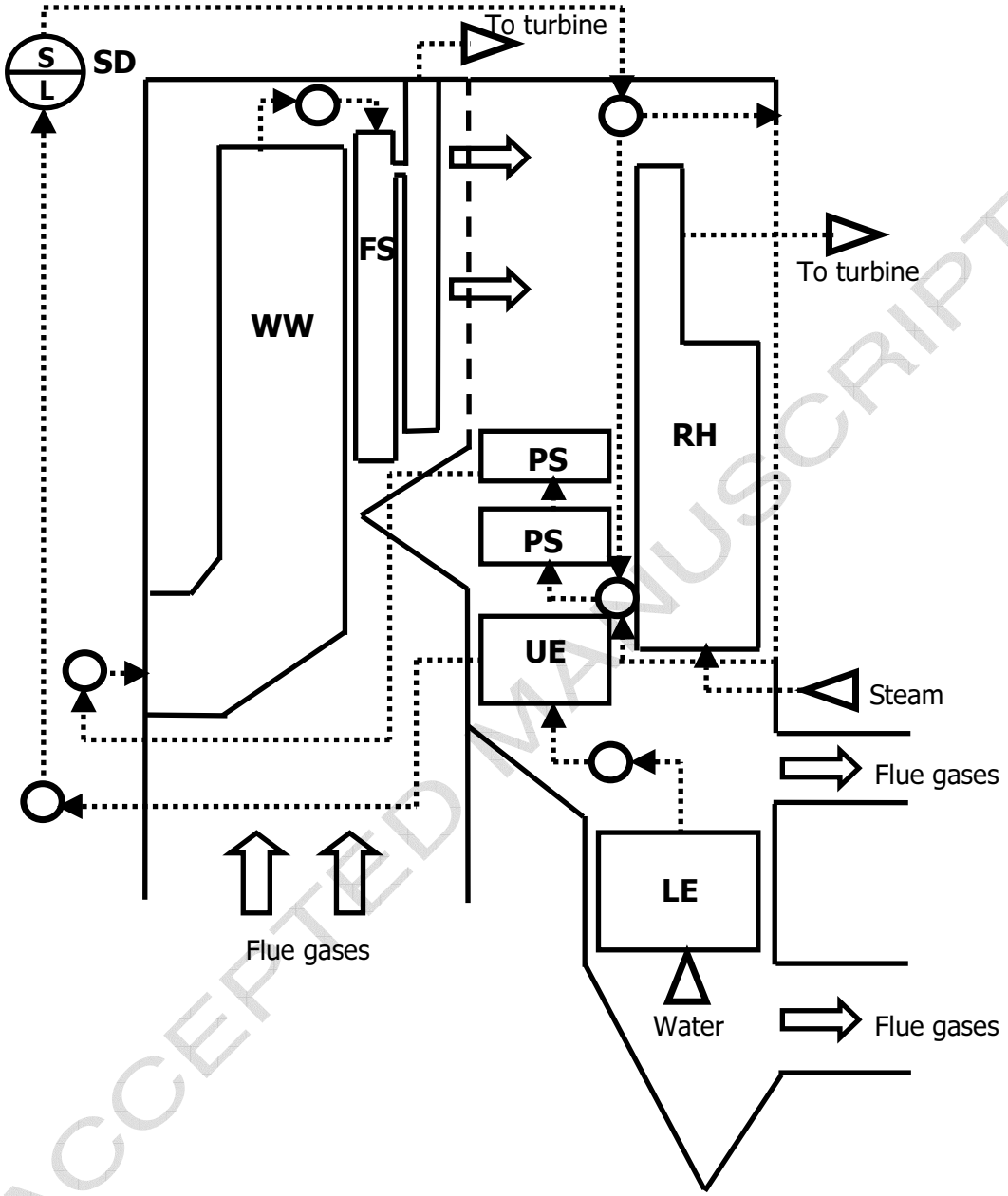

Fig. 3. Schematic of the simulated convective zone. Dotted lines indicate the circulation of the tube-side fluid between heat-exchanging elements. Triangles are inlet manifolds. Circles are intermediate manifolds. See text for nomenclature.

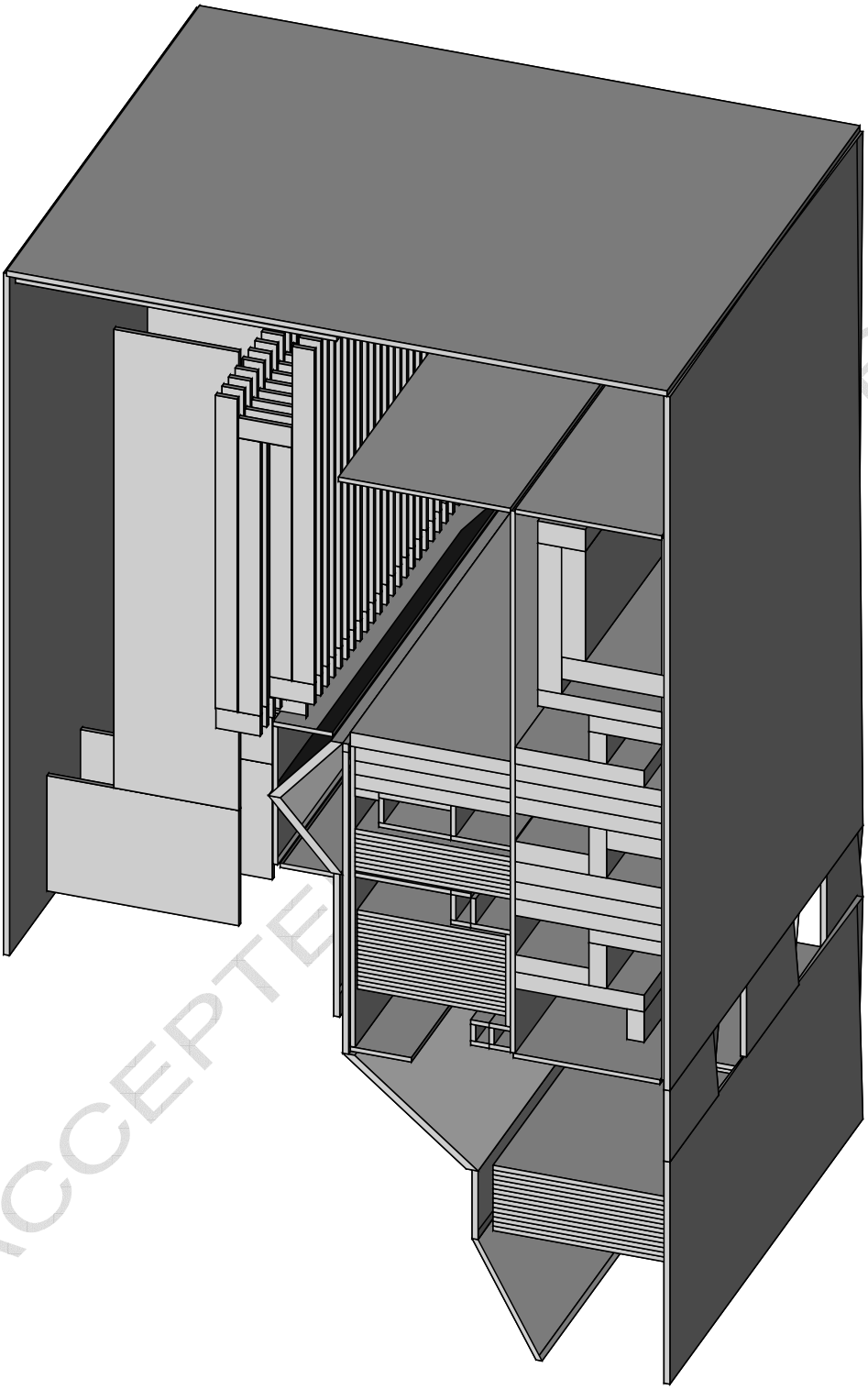

Fig. 4. Geometry of the convective zone, as represented in the model.

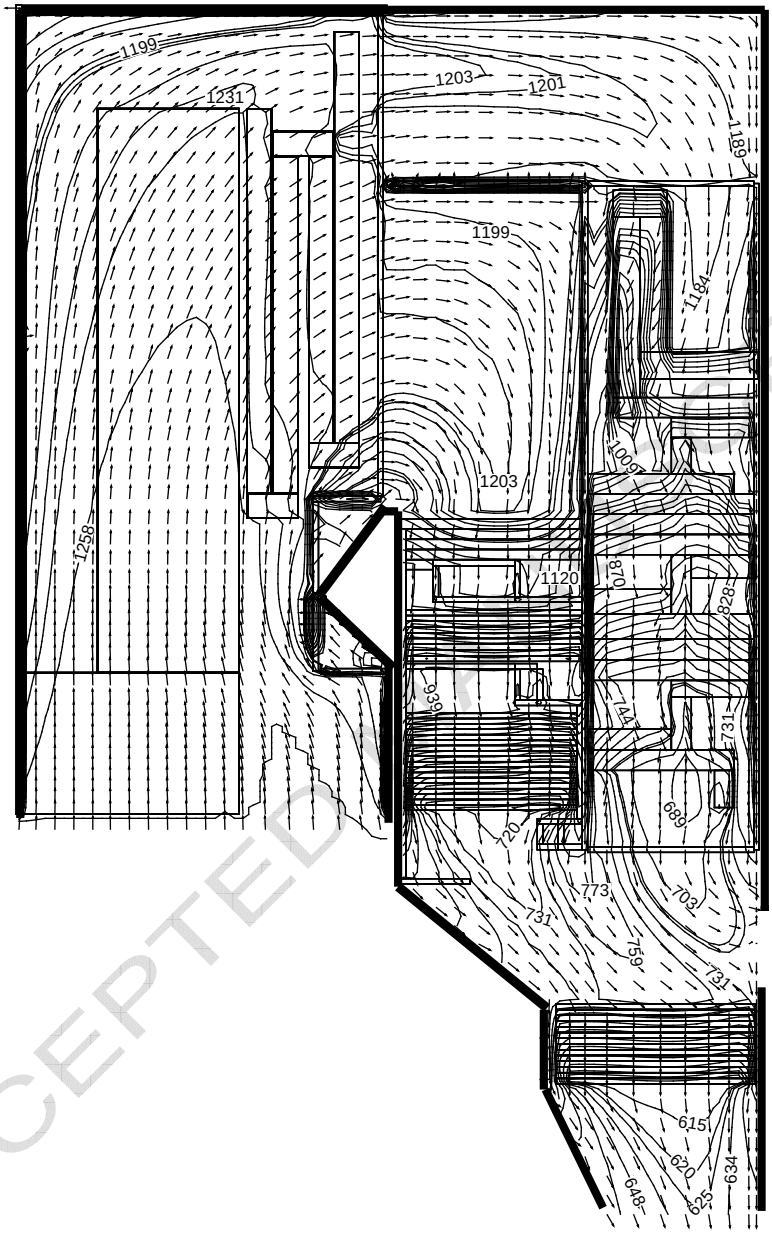

Fig. 5. Shell-side temperature and shell-side flow-field on a middle plane for 60% load.

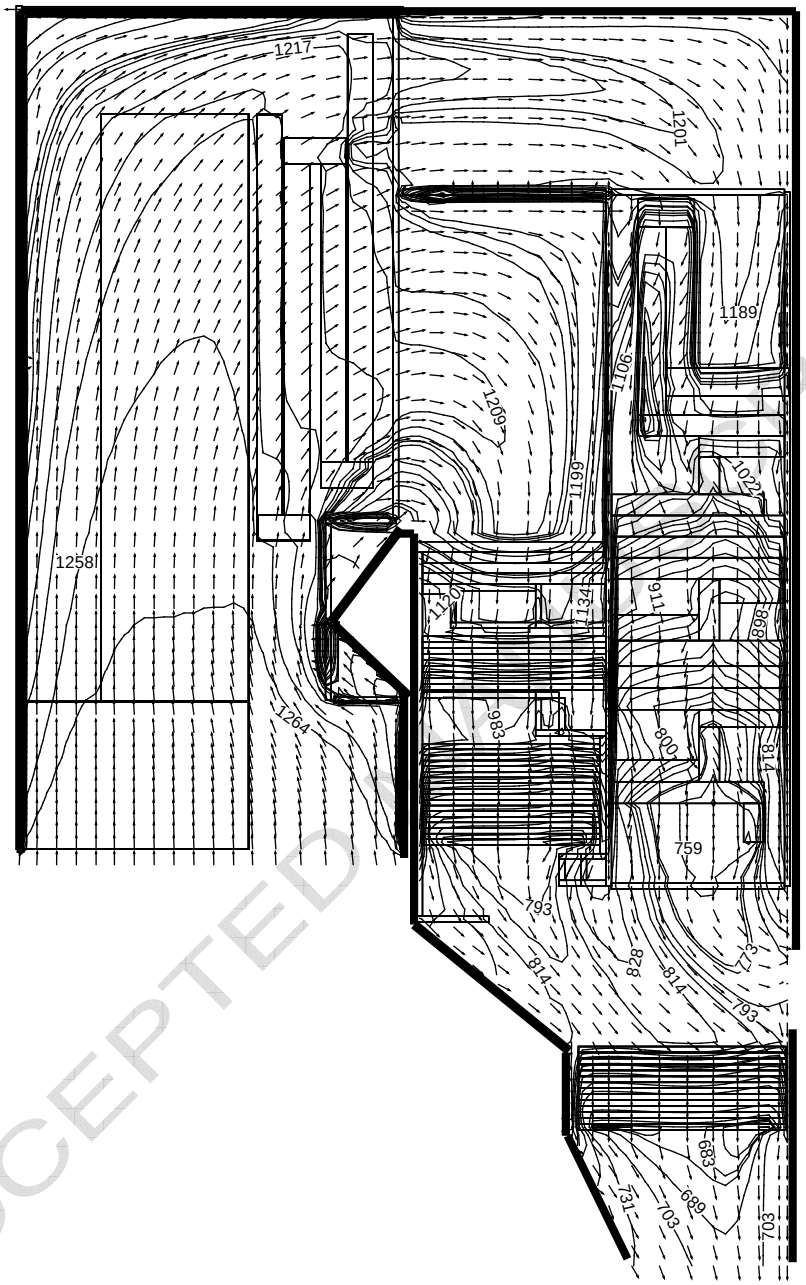

Fig. 6. Shell-side temperature and shell-side flow-field on a middle plane for 100% load.

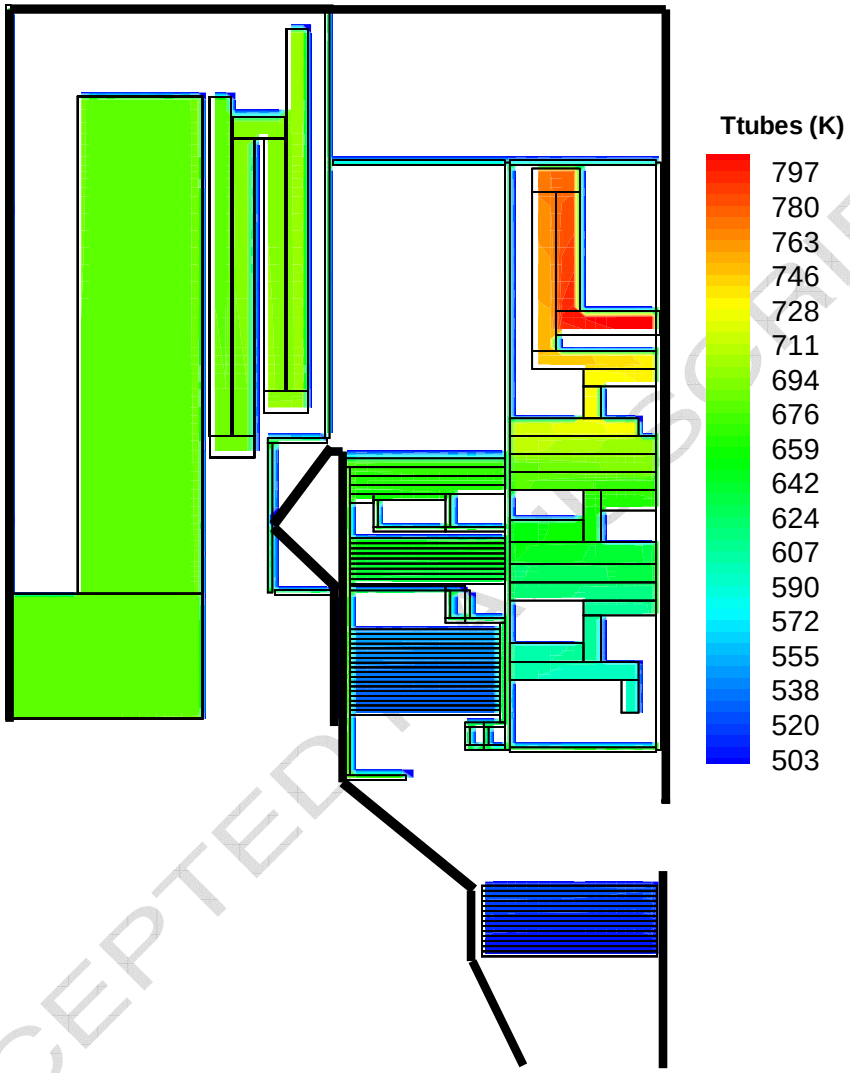

Fig. 7. Tube-side temperature on a middle plane for 60% load.

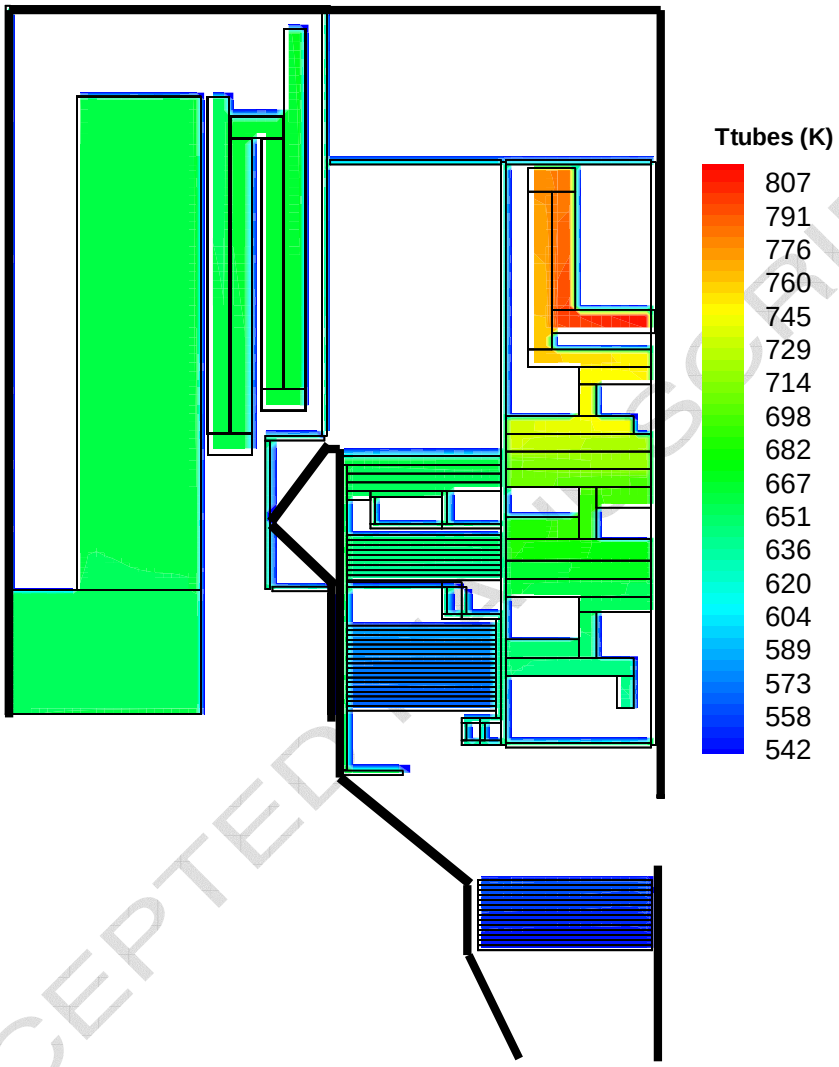

Fig. 8. Tube-side temperature on a middle plane for 100% load.

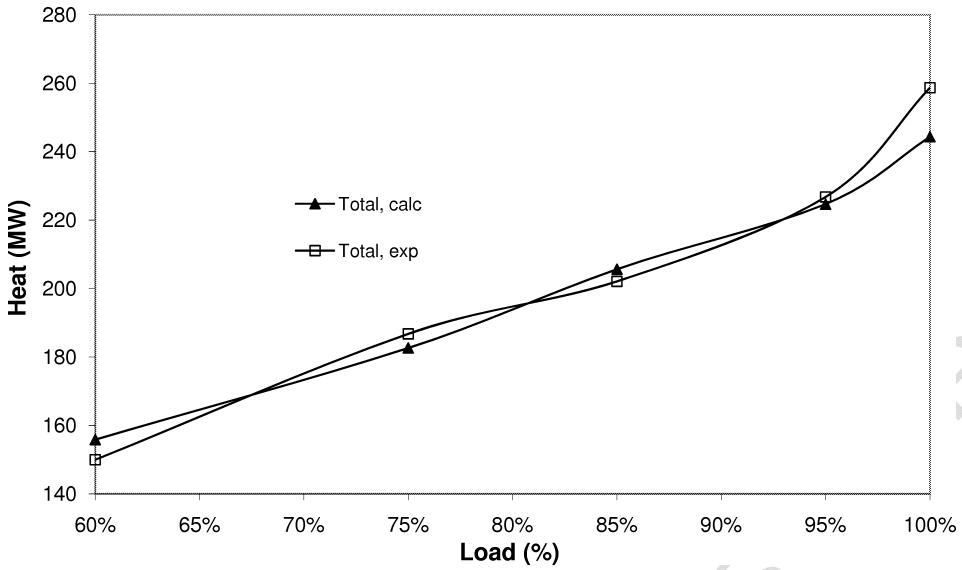

Fig. 9. Comparison between calculated and measured exchange heat for different loads.

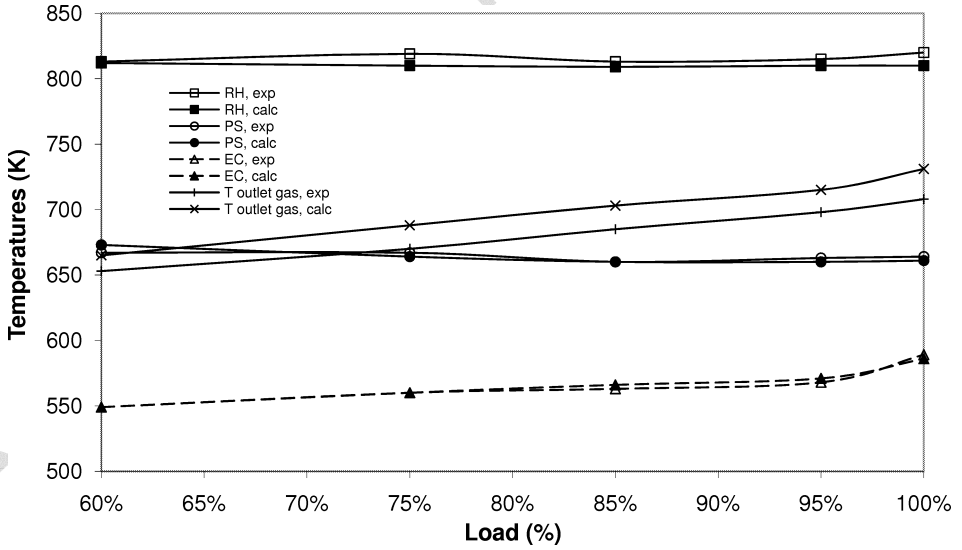

Fig. 10. Comparison between calculated and measured mean temperatures at the outlets of RH, PS, UE and the gas exit.